Solid-State Reaction Between Fe-Al-Ca Alloy and Al$_2$O$_3$-CaO-FeO Oxide During Heat Treatment at 1473 K (1200 °C)

CHENGSONG LIU, SHUFENG YANG, JINGSHE LI, HONGWEI NI, and XUELIANG ZHANG

The aim of this study was to control the physicochemical characteristics of inclusions in steel through appropriate heat treatment. Using a confocal scanning laser microscope (CSLM) and pipe furnace, the solid-state reactions between Fe-Al-Ca alloy and Al$_2$O$_3$-CaO-FeO oxide during heat treatment at 1473 K (1200 °C) and the influence of these reactions on the compositions of and phases in the alloy and oxide were investigated by the diffusion couple method. Suitable pretreatment of the oxide using a CSLM and production of the diffusion couple of Fe-Al-Ca alloy and Al$_2$O$_3$-CaO-FeO oxide gave good contact between the alloy and oxide. The diffusion couple was then sealed in a quartz tube with a piece of Ti foil to lower oxygen partial pressure and a block of Fe-Al-Ca alloy was introduced to conduct heat treatment experiments. Solid-state reactions between the alloy and oxide during heat treatment at 1473 K (1200 °C) were analyzed and discussed. A dynamic model to calculate the width of the particle precipitation zone based on the Wagner model of internal oxidation of metal was proposed. This model was helpful to understand the solid-state reaction mechanism between Fe-Al-Ca alloy and Al$_2$O$_3$-CaO-FeO oxide.

I. INTRODUCTION

GENERALLY, non-metallic inclusions in steel are mainly composed of deoxidation products. Non-metallic inclusions with high melting point and high hardness negatively affect the toughness, fatigue resistance, and ductility of steel. In the steel production process, complex deoxidizers, such as Si-Mn, Al-Ca, and Si-Mn-Al, are usually used to achieve deoxidation of molten steel and obtain compound deoxidization products with low melting points, which tend to aggregate, grow, and float upward.[1,2] Therefore, it is important to construct an appropriate equilibrium between molten steel and inclusions to improve steel quality and avoid the generation of simple non-metallic inclusions with high melting points such as Al$_2$O$_3$, CaO·2Al$_2$O$_3$, and SiO$_2$. In addition, the type, quantity, size, morphology, and various other physicochemical characteristics of final non-metallic inclusions that remain in steel after heat treatment and rolling directly affect the quality and properties of steel products. The final inclusions are often quite different from the initial ones in molten steel before solidification. Apart from reactions that occur during solidification as elements segregate, one of the main reasons for this is that the subsequent heat treatment process of cast billets not only influences the structure and properties of steel, but also changes the characteristics of non-metallic inclusions. Solid-state reactions between the steel and inclusions occur at high temperature, causing changes to the distribution of segregated elements, modification of original inclusions, and generation of new inclusions.

Takahashi et al.[3] studied the changes of the non-metallic inclusions in Fe-Cr-Ni alloys containing different contents of Si and Mn following heating at 1373 K and 1573 K (1100 °C and 1300 °C). After heating at 1373 K (1100 °C) for 1 hour, the MnO-SiO$_2$ inclusion changed to MnO-Cr$_2$O$_3$, while after heating at 1573 K (1300 °C) for 1 hour, the MnO-SiO$_2$ inclusion remained stable. Shibata et al.[4,5] investigated the solid-state reaction between Fe-Cr alloy and MnO-SiO$_2$ oxide during heat treatment at 1473 K (1200 °C) by the diffusion couple method. Their results showed that the critical Si content in the alloy at 1473 K (1200 °C) where the MnO-SiO$_2$-type inclusion changed to a MnO-Cr$_2$O$_3$-type inclusion was approximately 0.3 mass pct for 10 mass pct Cr steel. When the Si content was relatively high (>0.3 mass pct), the MnO-SiO$_2$-type inclusion was stable during heat treatment.

Shao and et al.[6] revealed the effect of heat treatment conditions on the shape control of large elongated MnS inclusions in resulfurized free-cutting steels. They found that as the heating time at 1473 K (1200 °C) was extended from 0 to 4 hours, the number density of MnS

CHENGSONG LIU, HONGWEI NI are with the The State Key Laboratory of Refractories and Metallurgy, Wuhan University of Science and Technology, Wuhan, 430081, China. SHUFENG YANG, JINGSHE LI, and XUELIANG ZHANG are with the School of Metallurgical and Ecological Engineering, University of Science and Technology Beijing, Beijing, 100083, China. Contact e-mail: yangshufeng@ustb.edu.cn.
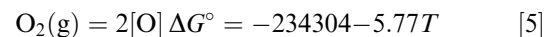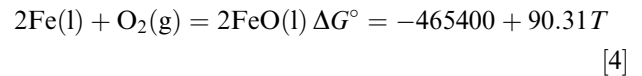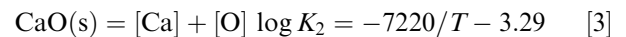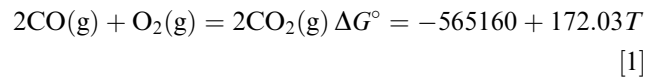
inclusions larger than 80 μm decreased from 1.91 to 0.46 mm^{-2}, while that of MnS inclusions smaller than 5 μm increased from 1322 to 6913 mm^{-2}. Thus, heat treatment at 1473 K (1200 °C) for 3 or 4 hours allows good shape and size control of large elongated MnS inclusions. The evolution of various inclusions in alloys deoxidized by Al and Ti during heat treatment at 1473 K (1200 °C) has also been investigated.[7] Original Al$_2$O$_3$, Al$_2$O$_3$-TiO$_x$, and TiO$_x$ inclusions in alloys with different Al and Ti contents gradually changed to Fe-Al-O, Fe-Al-Ti-O, and Fe-Ti-O inclusions during heat treatment.

Ohba et al.[8] determined the formation mechanism of oxide particles at surface cracks of Fe-0.8Mn-0.25-Si-1.1Cr alloy. They found that with sufficient heat treatment time at 1473 K and 1573 K (1200 °C and 1300 °C), the average sizes of oxide particles generated by internal oxidation gradually stabilized at 0.2 and 0.3 μm, respectively. These oxide particles were mainly composed of MnO-SiO$_2$ and MnO-Cr$_2$O$_3$ phases. First, a MnO-SiO$_2$ phase precipitated at the internal oxidation reaction front. Then, a MnO-Cr$_2$O$_3$ phase formed on the MnO-SiO$_2$ phase. The two phases played an important role in determining the final average size of oxide particles. A new approach to produce diffusion couples was developed to investigate the solid-state reaction between MnO-SiO$_2$-FeO oxide and Fe-Mn-Si alloy during heat treatment at 1473 K (1200 °C).[9] Compared with the experiment results obtained by Kim et al.,[10] the effect of pretreatment at 1673 K (1400 °C) on the diffusion experiment at 1473 K (1200 °C) was minimized by the new approach. As a result, the influence of oxygen diffusion on the solid-state reaction between the alloy and oxide during heat treatment at 1473 K (1200 °C) was observed clearly.

The above studies indicate that it is feasible to control the physicochemical characteristics of non-metallic inclusions by appropriate heat treatment. Aluminum deoxidation technology and calcium treatment are widely used in the modern steelmaking process. Physicochemical characteristics of Al-Ca-type inclusions formed in steel are probably changed by heat treatment. However, previous studies have mainly focused on the modification of Mn-Si-, Mn-Cr-, and Al-Ti-type inclusions by heat treatment. Little attention has been paid to the solid-state reaction between Al-Ca-type inclusions and Fe-Al-Ca alloy, which drives modification of Al-Ca-type inclusions in this alloy during heating. In addition, the transformation between different Al-Ca-type oxide compounds during heat treatment is still unclear. In this study, the equilibrium between Fe-Al-Ca alloy and Al$_2$O$_3$-CaO-FeO oxide at 1873 K (1600 °C) is first established. Then, solid-state reactions between this alloy and oxide during heat treatment at 1473 K (1200 °C) and their influence on the compositions and phases in the alloy and oxide are investigated by a new diffusion couple method. The findings allow the reaction mechanism to be clarified and discussed. Finally, a dynamic theoretical model to calculate the width of the particle precipitation zone (PPZ) is proposed to quantitatively analyze the solid-state reaction degree between this alloy and oxide.

II. EQUILIBRIUM BETWEEN THE ALLOY AND OXIDE AT 1873 K (1600 °C)

Figure 1 depicts the experiment apparatus used to estimate the equilibrium compositions of Fe-Al-Ca alloy and Al$_2$O$_3$-CaO-FeO oxide at 1873 K (1600 °C). Electrolytic Fe, Al metal, and Ca metal were melted in an arc melting furnace at 1873 K (1600 °C) for 30 minutes to produce Fe-Al-Ca alloy. The yield rates of Al and Ca metal during making the alloy were about 72 and 55 mass pct, respectively. Al$_2$O$_3$-CaO-FeO was prepared by mixing chemically pure Al$_2$O$_3$, CaO, and FeO in a pipe furnace at 1873 K (1600 °C) for 60 minutes. The quantities of the alloy and oxide prepared for subsequent experiments were 6 kg and 200 g, respectively. A Pt-6 pct Rh/Pt-30 pct Rh thermocouple was used to measure the temperature of the samples, which was maintained within ±5 K of the target value. An Al$_2$O$_3$ crucible with an inner diameter of 30 mm and height of 80 mm was charged with the oxide (about 10 g) and alloy (20 g). In the experiment, 12CaO·7Al$_2$O$_3$ with low melting point and high sulfur capacity was chosen as the target equilibrium composition of the oxide. CO and CO$_2$ gas flows, which were 1.65 × 10^{-4} and 1.5 × 10^{-6} m^3/min, respectively, were used to control the oxygen partial pressure. Considering the influence of oxygen partial pressure on deoxidization of molten steel by Al and Ca, FeO was likely to become one of the components of inclusions.[11,12] To determine the initial slag and alloy compositions, the equilibrium relation between the Al$_2$O$_3$-CaO-FeO oxide and Fe-Mn-Si alloy at 1873 K (1600 °C) was calculated using Eq. [1]-[7].[13–15]

$$2CO(g) + O_2(g) = 2CO_2(g) \quad \Delta G^\circ = -565160 + 172.03T \tag{1}$$

$$Al_2O_3(s) = 2[Al] + 3[O] \quad \log K_1 = -47400/T + 12.32 \tag{2}$$

$$CaO(s) = [Ca] + [O] \quad \log K_2 = -7220/T - 3.29 \tag{3}$$

$$2Fe(l) + O_2(g) = 2FeO(l) \quad \Delta G^\circ = -465400 + 90.31T \tag{4}$$

$$O_2(g) = 2[O] \quad \Delta G^\circ = -234304 - 5.77T \tag{5}$$

$$3[Ca] + Al_2O_3(s) = 3CaO(s) + 2[Al] \quad \log K_3 = -15661/T + 2.58 \tag{6}$$

$$K_3 = \left[a_{CaO(s)}/a_{Ca}\right]^3 \cdot \left[a_{Al}\right]^2 / a_{Al_2O_3(s)} \tag{7}$$
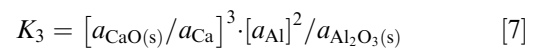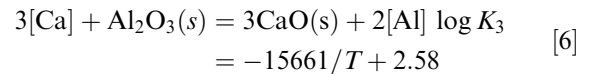
In these equations, a pure substance was selected as the standard state of the oxide. $a_{Al_2O_3(s)}$ and $a_{CaO(s)}$ represent the activities of Al$_2$O$_3$ and CaO in the oxide, respectively. a_{Al} and a_{Ca} represent the activities of Al

and Ca in the alloy, whose standard states were selected as solutions with 1 mass pct of Al and Ca, respectively. To observe the equilibration process and reach the equilibrium composition in a short time, the initial Al_2O_3-CaO-FeO oxide was not saturated with Al_2O_3, and the initial Fe-Al-Ca alloy was close to the equilibrium composition. The partial pressure of oxygen, initial compositions used in experiments, and calculated equilibrium compositions of the alloy and oxide determined using the above equations are listed in Table I.

During the experiment, the holding times of the samples in the furnace of 20, 40, 60, and 80 minutes were investigated. The contents of Al, Ca, and Fe elements in the oxide were analyzed by inductively coupled plasma-atomic emission spectroscopy. The composition of the alloy was analyzed by electron probe microanalysis (EPMA). Figure 2 shows the changes in the compositions of the alloy and oxide with holding time at 1873 K (1600 °C). In each case, the equilibrium is achieved within 20 minutes. The experimental results are in good agreement with the calculation data. The equilibrium oxide was not a binary oxide of Al_2O_3-CaO but a ternary oxide containing 0.5 mass pct FeO. This result could reflect the equilibrium state between Fe-Al-Ca and Al_2O_3-CaO-FeO effectively and provide reliable initial compositions of the alloy and oxide for subsequent

Fig. 1—Experiment apparatus used for estimating the equilibrium compositions of Fe-Al-Ca alloy and Al_2O_3-CaO-FeO oxide.

1. Gas Inlet
2. Thermocouple
3. Si Rubber Stopper
4. Alumina Tube
5. Heating element
6. Fe-Al-Ca Alloy
7. Al_2O_3-CaO-FeO oxide
8. Alumina Crucible
9. Mo holder
10. Quartz Tube
11. Gas Outlet
12. Sealing Cap
13. View Window

investigation of the solid-state reactions between them during heat treatment at 1473 K (1200 °C).

III. REACTION BETWEEN THE ALLOY AND OXIDE DURING HEAT TREATMENTS 1473 K (1200 °C)

A. Experimental Method

In this study, equilibrium compositions of Fe-Al-Ca and Al_2O_3-CaO-FeO at 1873 K (1600 °C) (see Table I) were chosen as the initial compositions to prepare the diffusion couple. Using a planetary ball mill, the oxide was firstly grinded to powder (~100 μm) with absolute ethyl alcohol as mill mediator and then sampled by quartering method. To obtain good contact between the alloy and oxide, the oxide powder was melted at 1700 K (1427 °C) in a confocal scanning laser microscope (CSLM; VL2000DX-SVF17SP, Lasertec Corporation, Japan). The alloy was machined into an approximate cylinder ($\varnothing 5 \times 3$ mm) containing a small circular hole ($\varnothing 1.5$ mm) for the oxide powder (~25 mg). The alloy and oxide powder were inserted into an Al_2O_3 crucible with an inner diameter of 8 mm and height of 3.5 mm. Figure 3 shows the experimental set-up for melting the oxide contained in the alloy cylinder in the CSLM. After evacuating the CSLM chamber to 5.0×10^{-3} Pa, pure argon gas was introduced to protect the samples from oxidation. The temperature was increased from room temperature to about 1700 K (1427 °C) (20 K higher than the melting point of the oxide) at a rate of 100 K/min. When the oxide had melted, the sample was quenched immediately at a rate of about 1000 K/min to suppress the reaction between the alloy and oxide at this point and improve the homogeneity of the re-melted oxide.

After oxide pre-melting in the CSLM, the diffusion couple specimen, a piece of Ti foil used to decrease oxygen partial pressure and a block of alloy with the same composition as that in the diffusion couple specimen were sealed in a quartz tube filled with pure argon gas at a pressure of about 2×10^4 Pa, as shown in Figure 4. The bulk alloy was used to separate the diffusion couple specimen from the Ti foil and avoid the contamination of titanium oxide products. The whole quartz tube was then heated in a pipe furnace at a controlled temperature. In this study, the heat treatment temperature was set at 1473 K (1200 °C) and the holding times were 10 and 50 hours. The temperature curve for the heat treatment of the diffusion couple
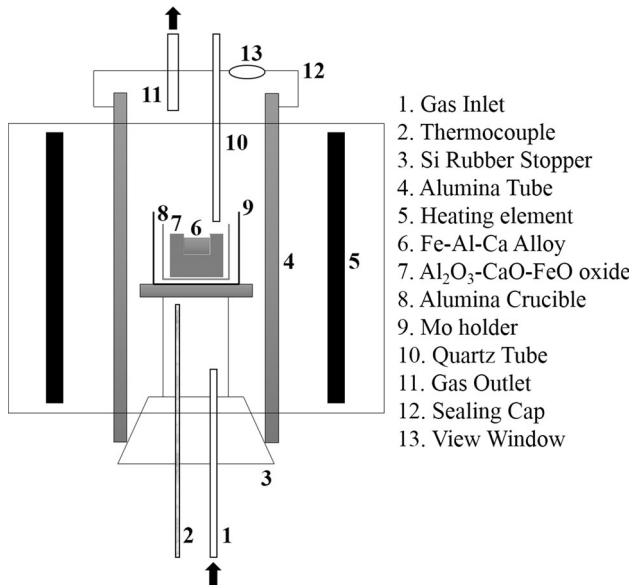
Table I. Partial Pressure of Oxygen, Initial Compositions in the Experiment, and Calculated Equilibrium Compositions of the Alloy and Oxide at 1873 °C (1600 °C)

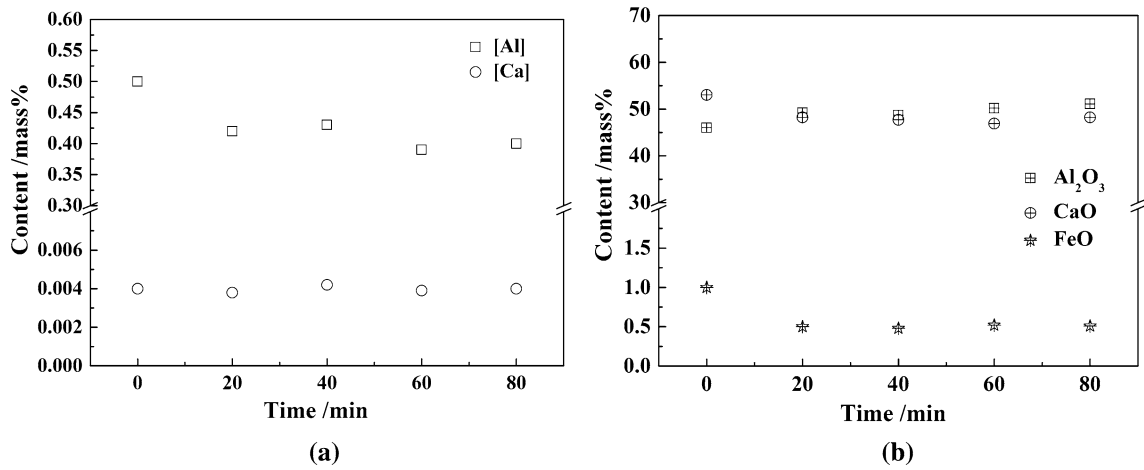|	Alloy (Mass Pct)			Oxide (Mass Pct)			
	Fe	Al	Ca	Al_2O_3	CaO	FeO	P_{O_2}
Calculated equilibrium	bal.	0.4	0.004	51.26	48.24	0.50	1.4×10^{-13}
Initial	99.5	0.5	0.004	46.00	53.00	1.00	1.4×10^{-13}

Fig. 2—Equilibrium experiment results at 1873 K (1600 °C). (*a*) Change in the composition of the alloy with time; (*b*) Change in the composition of the oxide with time.
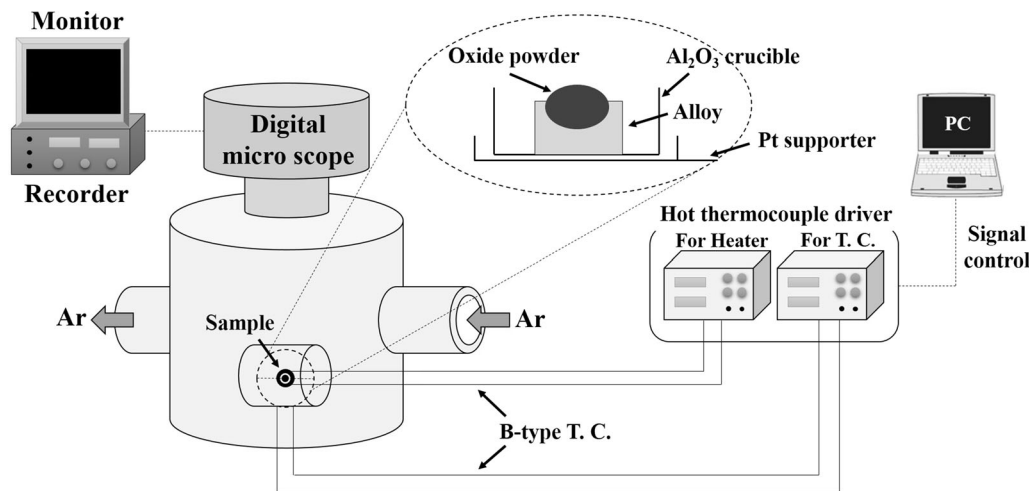

Fig. 3—Experimental set-up for melting the oxide in CSLM.

specimen is displayed in Figure 5. Here, G-0, G-10, and G-50 refer to the specimens after oxide pre-melting and after heat treatment for 10 and 50 hours, respectively. After heat treatment, the quartz tube was quenched with water. A vertical cross section of each quenched diffusion couple was mirror-polished. Then, the morphology and chemical composition of the alloy and oxide at the alloy–oxide interface in diffusion couple G-0, G-10, and G-50 were analyzed by EPMA.

To avoid the oxide particles that precipitated in the alloy near the alloy–oxide interface affecting the measurement of alloy composition, standard samples were used to calibrate the element contents in the alloy during EPMA each time. Moreover, Eq. [8] was used to deal with the compositions of oxide particles in the alloy,[4]

$$C_{M,oxide} = C_{M,analysis} - C_{Fe,analysis}/C_{Fe,steel} \times C_{M,steel}, \quad [8]$$

where $C_{M,oxide}$ and $C_{M,analysis}$ indicate the contents of element M in the oxide and in the analyzed area, respectively; $C_{Fe,analysis}$ and $C_{Fe,steel}$ indicate the
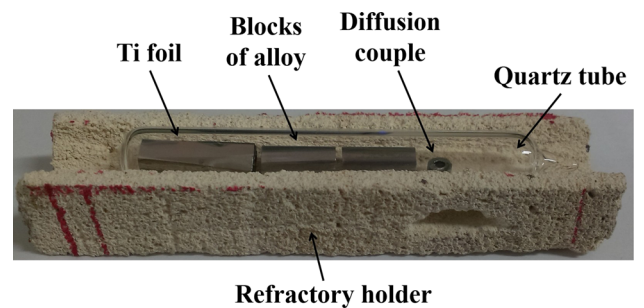

Fig. 4—Schematic of the diffusion couple specimen sealed in a quartz tube.

contents of Fe in the analyzed area and in the alloy matrix, respectively; and $C_{M,steel}$ indicates the content of element M in the alloy matrix. In Eq. [8], it was assumed that all of the Fe in the analyzed area came from the alloy matrix. Al and Ca that came from the alloy matrix were calculated from the ratios of Al/Fe and Ca/Fe in the initial alloy matrix. The content of

each element in the oxide was determined by the difference between the calculated and the analyzed values. Mass fractions of Al_2O_3, CaO and FeO were obtained by direct conversion from the contents of Al, Ca, and Fe in the oxide.

Fig. 5—Temperature curve of the heat treatment for the diffusion couple specimen.

B. Experimental Results for Heat Treatment

Figure 6 shows the interface of the alloy and oxide in diffusion couples G-0, G-10, and G-50. Tables II, III, and IV report the chemical composition analysis of positions shown in Figures 6(a) through (c), respectively. Figure 6(a) reveals that after heating at 1700 K (1427 °C), good contact was obtained between the Fe-Al-Ca alloy and Al_2O_3-CaO-FeO oxide. Some gray particles and dendritic inclusions precipitated in the alloy near the alloy–oxide interface after heat treatment at 1473 K (1200 °C). Several phases are also observed in the oxide. The EPMA results in Table II indicate that the main component of the gray particles is Al_2O_3, and that of the dendritic inclusions is close to $CaO \cdot Al_2O_3$. The quantities and scales of the two products were positively correlated with heat treatment time. In all cases, the main component of the main gray phase in the oxide was $12CaO \cdot 7Al_2O_3$. After heating at 1700 K (1427 °C), a white phase with high FeO content (>31.0 mass pct) was found in the oxide. After heat treatment at 1473 K (1200 °C) for 10 and 50 hours, the white phase in the oxide gradually turned into particles of various sizes (Figures 6(b) and (c)). According to the chemical composition analysis in Tables III and IV, the
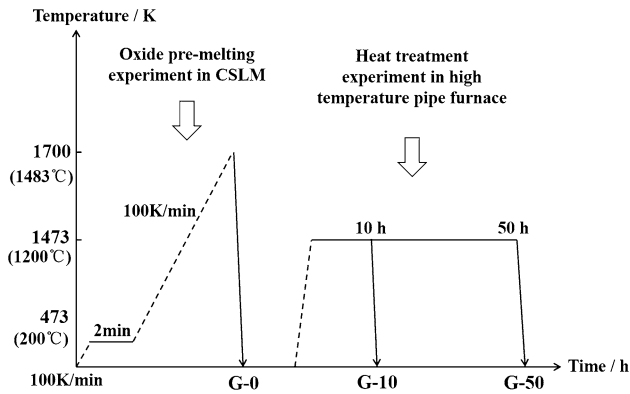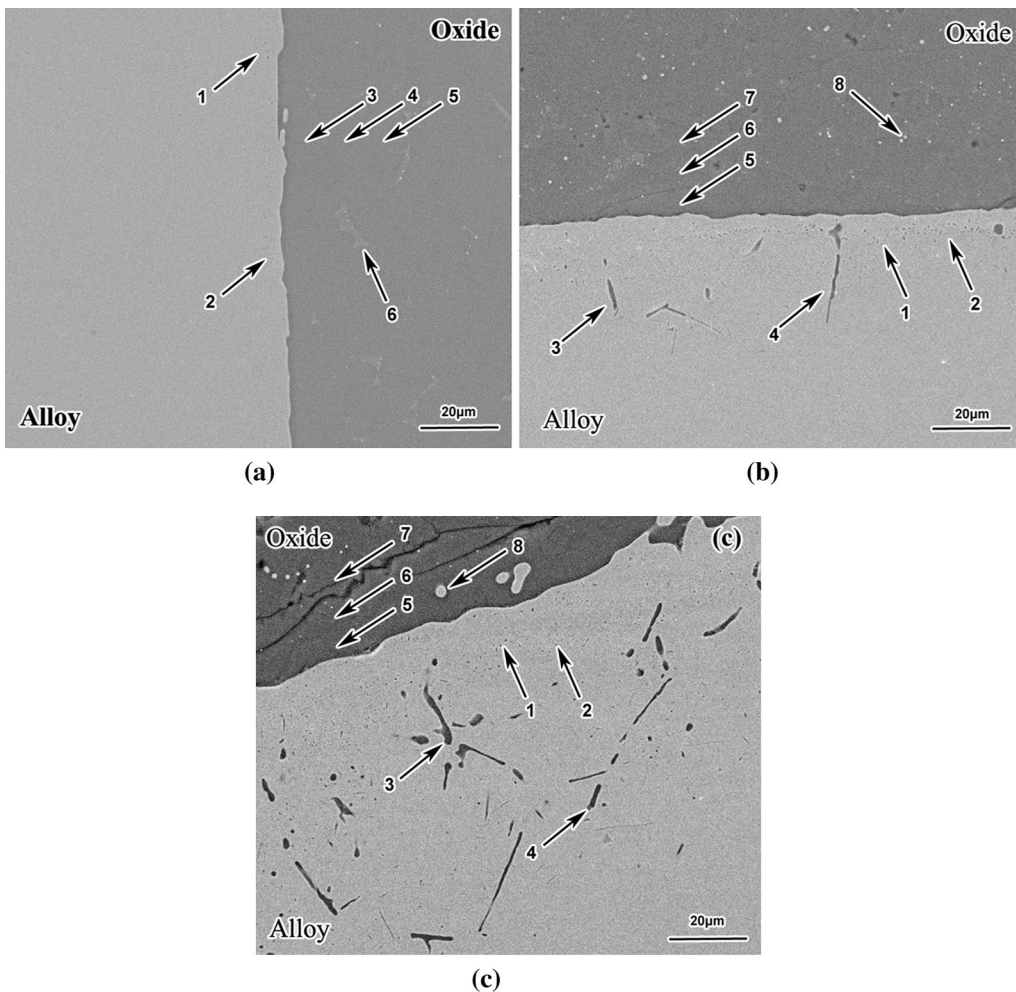

Fig. 6—Interface of the alloy and oxide in the diffusion couple of G-0, G-10, and G-50. (a) G-0; (b) G-10; (c) G-50.

Table II. Chemical Composition Analysis of Positions in Fig. 6(a)

Phase	Position	Mass Pct		
		Al$_2$O$_3$	CaO	FeO
Particle	1	99.2	0.8	0
	2	99.4	0.6	0
Oxide	3	51.4	48.0	0.6
	4	52.7	46.9	0.4
	5	51.9	47.6	0.5
	6	35.6	32.8	31.6

Table III. Chemical Composition Analysis of Positions in Fig. 6(b)

Phase	Position	Mass Pct		
		Al$_2$O$_3$	CaO	FeO
Particle	1	99.5	0.5	0
	2	99.7	0.3	0
	8	Fe: 74.2, Al: 10.3, Ca: 13.1, O: 2.4		
Branch	3	70.2	29.8	0
	4	61.9	38.1	0
Oxide	5	51.8	47.9	0.3
	6	50.9	48.9	0.2
	7	52.1	47.5	0.4

Table IV. Chemical Composition Analysis of Positions in Fig. 6(c)

Phase	Position	Mass Pct		
		Al$_2$O$_3$	CaO	FeO
Particle	1	99.6	0.4	0
	2	99.5	0.5	0
	8	Fe: 95.6, Al: 2.1, Ca: 1.8, O: 0.5		
Branch	3	62.9	37.1	0
	4	64.1	35.9	0
Oxide	5	52.4	47.5	0.1
	6	51.7	48.1	0.2
	7	52.1	47.8	0.1

Fe content in the white phase rose constantly with lengthening heat treatment time up to >95.0 mass pct after heat treatment for 50 hours. The contents of Al$_2$O$_3$ and CaO in the gray phase of the oxide were relatively stable, while the FeO content gradually decreased with extending heat treatment period.

Figure 7 shows the Al and Ca contents in the alloy near the alloy–oxide interfaces of diffusion couple G-0, G-10, and G-50. After heating at 1700 K (1427 °C), some chemical reaction between the alloy and oxide occurred, which caused the Al content to decrease and Ca content to increase in the alloy close to the alloy–oxide interface. Here, the region in which the Al content is lower than that in the bulk alloy is defined as the Al-depleted zone (ADZ). Similarly, the region in which the Ca content is higher than that in the bulk alloy is defined as the Ca-accumulated zone (CAZ). After heat treatment at 1473 K (1200 °C) for 10 hours, moving gradually toward the alloy–oxide interface, the Al content decreased from 0.4 to about 0.05 mass pct and Ca content increased from 0.004 to 0.28 mass pct. When the heat treatment time was extended to 50 hours, ADZ width became larger while the CAZ width remained almost stable. The minimum Al content and maximum Ca content after heat treatment for 50 hours were about 0.012 and 0.26 mass pct, respectively. Unlike a previous study on the solid-state reaction between Fe-Mn-Si alloy and MnO-SiO$_2$-FeO oxide,[9] there was no slight increase of Al content in the alloy close to the alloy–oxide interface.

Figure 8 displays the PPZ and ADZ widths of diffusion couple G-0, G-10, and G-50. In this study, the method used to calculate PPZ width was the same as that defined in Reference 10, even though some dendritic inclusions also precipitated in the alloy near the alloy–oxide interface. The PPZ and ADZ widths possess a positive logarithm function correlation which is shown in Figure 8. The width of ADZ was always larger than that of the PPZ after heat treatment at 1473 K (1200 °C). As the heat treatment time was lengthened from 0 to 10 to 50 hours, PPZ width increased from 10 to 31 to 87 μm, respectively, while ADZ width increased from 7 to 31 to 170 μm, respectively.

Figure 9 depicts the size distribution of the gray particles in the PPZ of the diffusion couples before and after heat treatment at 1473 K (1200 °C). The scales of dendritic inclusions that precipitated in the alloy near the alloy–oxide interface were converted into equivalent diameters according to their areas determined by EPMA. The results suggest that the particle size can be divided into two categories: <0.5 and >0.5 μm. As heat treatment time increased from 0 to 10 to 50 hours, the number of particles smaller than 0.5 μm per 2500 μm^2 first increased and then decreased. The number of larger particles (>0.5 μm) per 2500 μm^2 basically increased with extending heat treatment time, especially the number of particles larger than 3.0 μm, which was mainly caused by the precipitation of dendritic inclusions in the alloy.

Figure 10 presents the compositions of the gray particles and the dendritic inclusions precipitated in the PPZ of the alloy near the alloy–oxide interface before and after heat treatment, which are plotted in the ternary phase diagram of the Al$_2$O$_3$-CaO-FeO system at 1473 K (1200 °C). It is clear that the composition of particle inclusions is close to pure Al$_2$O$_3$ and that of dendritic inclusions is located around CaO·Al$_2$O$_3$. It can be inferred that through solid-state reaction between the Fe-Al-Ca alloy and Al$_2$O$_3$-CaO-FeO oxide during heat treatment, Al$_2$O$_3$ and CaO·Al$_2$O$_3$ inclusions with high melting points and relatively low sulfur capacities are formed even though the initial 12CaO·7Al$_2$O$_3$ oxide is in a liquid state at 1873 K (1600 °C).

C. Discussion

1. Mechanism of the solid-state reaction

The experimental evidence indicates the precipitation of Al$_2$O$_3$ particle inclusions and CaO·Al$_2$O$_3$ dendritic inclusions in the alloy near the alloy–oxide interface,
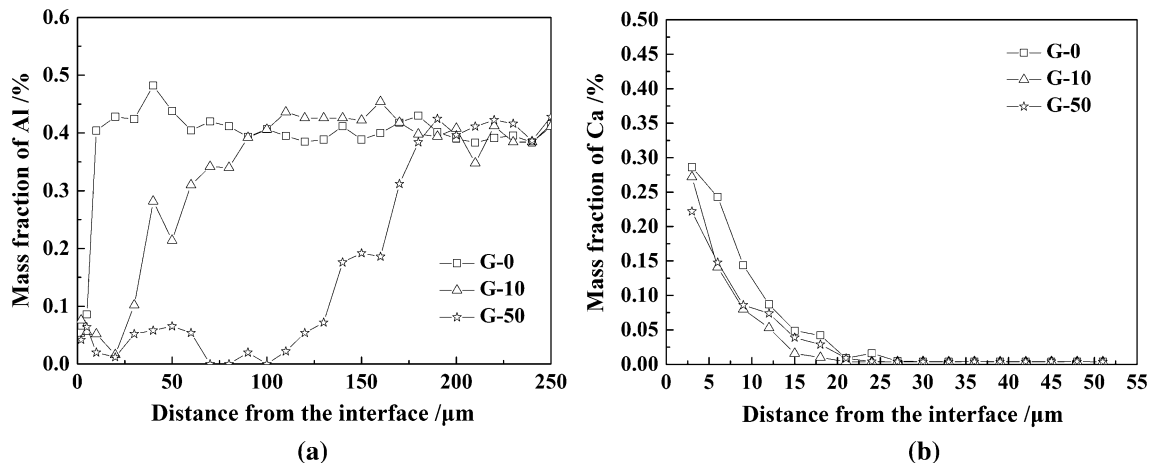
(a)

(b)

Fig. 7—Change of Al and Ca contents in the alloy before and after heat treatment at 1473 K (1200 °C). (*a*) Al content; (*b*) Ca content.
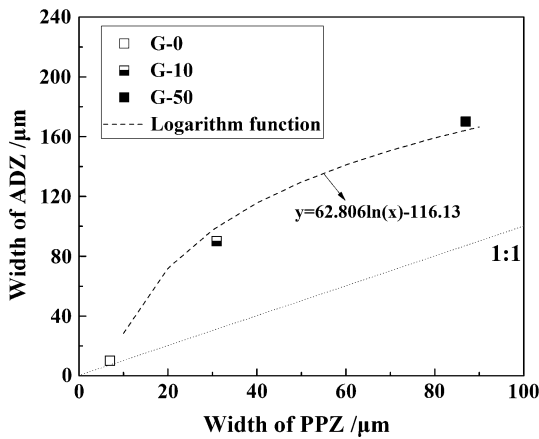

Fig. 8—PPZ and ADZ widths in the diffusion couple before and after heat treatment at 1473 K (1200 °C).
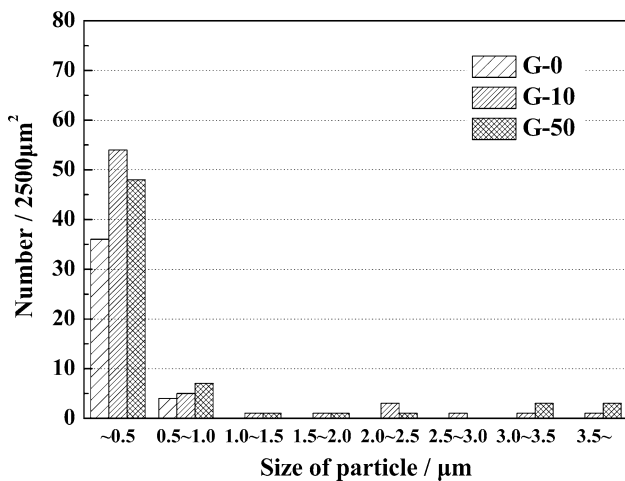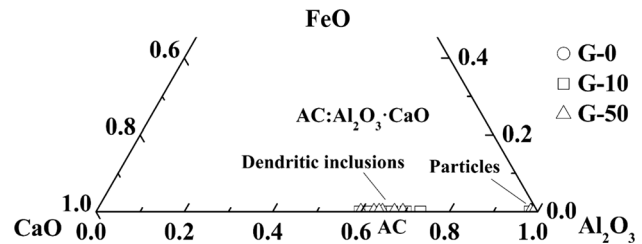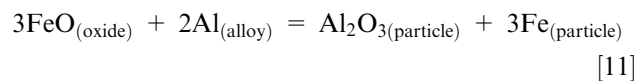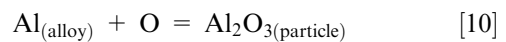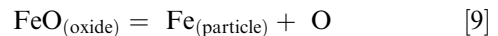

Fig. 10—Compositions of the gray particles and dendritic inclusions in the PPZ before and after heat treatment at 1473 K (1200 °C).

decreased to 1473 K (1200 °C), the alloy and oxide in the diffusion couples became non-equilibrated and solid-state reactions occurred between them. Because of the lack of thermodynamic data for these solid-state reactions, the basic thermodynamic data at 1873 K (1600 °C) were extended to lower temperature to calculate the activities of oxygen in the alloy and FeO in the oxide, which was in equilibrium with Fe-0.4 mass pct Al-0.004 mass pct Ca alloy, at 1700 K and 1473 K (1427 °C and 1200 °C). The results of this calculation are presented in Figure 11. As the temperature decreased from 1873 K to 1700 K to 1473 K (from 1600 °C to 1427 °C to 1200 °C), oxygen activity in the alloy decreased from 0.00097 to 0.00027 to 0.000054, respectively, and FeO activity in the oxide decreased from 0.0049 to 0.0034 to 0.0021, respectively. During heat treatment at 1473 K (1200 °C), FeO in the oxide decomposed into pure metallic particles and elemental O, then the latter diffused from the oxide into the alloy and reacted with elemental Al, which caused the precipitation of Al_2O_3 particle inclusions near the alloy–oxide interface. The involved chemical reactions are expressed by Eqs. [9]-[11].
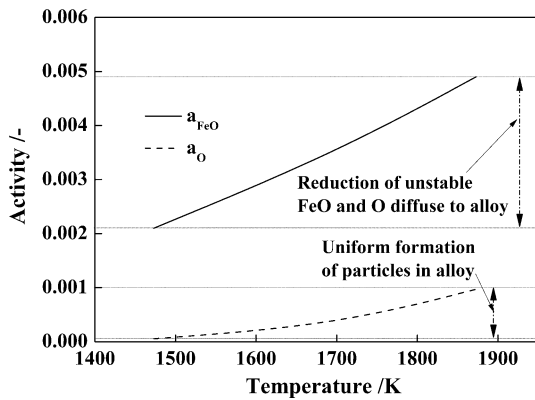
$$FeO_{(oxide)} = Fe_{(particle)} + O \qquad [9]$$

$$Al_{(alloy)} + O = Al_2O_{3(particle)} \qquad [10]$$

$$3FeO_{(oxide)} + 2Al_{(alloy)} = Al_2O_{3(particle)} + 3Fe_{(particle)} \qquad [11]$$

Fig. 9—Size distribution of the gray particles in the PPZ of the diffusion couple before and after heat treatment at 1473 K (1200 °C).

which results in the formation of ADZ and CAZ. Therefore, even though an equilibrium state between the Fe-Al-Ca alloy and Al_2O_3-CaO-FeO oxide was confirmed at 1873 K (1600 °C), as the temperature

Fig. 11—Change of activity of oxygen and FeO with temperature in equilibrium calculation.

Fig. 12—Schematic of the formation mechanism of the particles and dendritic inclusions in the alloy near the interface.

Furthermore, $12CaO \cdot 7Al_2O_3$ phase in the oxide was not stable at high temperature and also tended to react with Al element in the alloy at the alloy–oxide interface.[16] This chemical solid-state reaction can be expressed by Eq. [12]. Because of this type of solid-state reaction, on the one hand, $CaO \cdot Al_2O_3$-type dendritic inclusions precipitated in the alloy near the alloy–oxide interface, and on the other hand, Al and Ca contents in the alloy decreased and increased, respectively. Figure 12 summarizes the formation mechanism of particles and dendritic inclusions in the alloy near the alloy–oxide interface.

$$4(12CaO \cdot 7Al_2O_3) + 10Al = 15Ca + 33(CaO \cdot Al_2O_3) \quad [12]$$
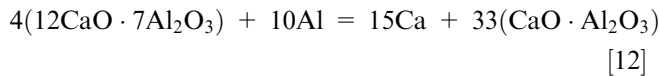
In addition, as shown in Figure 13, the activity coefficients of Al, Ca, O in the alloy, and FeO in the oxide before and after the heat treatment at 1473 K (1200 °C) for 10 and 50 hours have been calculated. Activity coefficients for Al, Ca, and O in the alloy were assumed to be a unit from Henry's Law in solid iron; activity coefficient of FeO in the oxide was obtained by using regular solution model.[17] Contents of Al, Ca in the alloy, and FeO in the oxide were obtained according to the experiment results before and after the heat treatment. O content in the alloy was calculated by using Eqs. [4] and [5] at 1473 K (1200 °C), although these values are valid only for the liquid state. From Figure 13, it could be observed that with the increase of heat treatment time, the activities of Al and O in the alloy and FeO in the oxide decreased while the activity of Ca in the alloy increased. All gradients in the activities of Al, Ca, O, and FeO tended to became lower after long heating which indicated that the system approached equilibrium state.

By the mechanism of the solid-state reaction between the alloy and oxide, the mass of Al decreased in the alloy near interface should correspond with the mass of Al precipitated as oxide particles. To confirm this, a rough calculation was carried out. The decrease of the average Al content in ADZ is assumed to be x pct and the mass of ADZ is "W (kg)," the mass of decreased Al is calculated as "$W \cdot x/100$ (kg)." Assuming the radius of
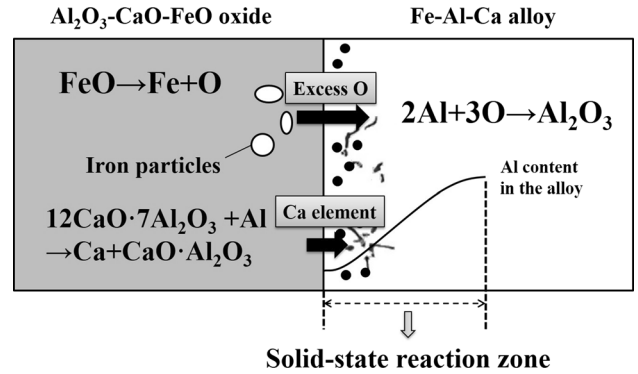
spherical Al_2O_3 or $CaO \cdot Al_2O_3$ oxide to be r_1 (m), the number of precipitated oxide was set to be "n_1." The total mass of Al ("P, kg") which consumed to form Al_2O_3 particle inclusions and $CaO \cdot Al_2O_3$-type dendritic inclusions can be calculated as Eq. [13], where ρ_1 is density of oxide (4182 kg/m³). The density of steel is assumed to be ρ_2 (7850 kg/m³).

$$P = n \cdot \frac{4}{3} \cdot \pi \cdot r^3 \cdot \rho_1 \cdot \left(\frac{27 \times 2}{27 \times 2 + 16 \times 3} \right) = \frac{W \cdot x}{100}. \quad [13]$$

By this equation, the density of the oxide particles in ADZ was calculated as "n/W, 1/kg-Fe." The number of particles per 1000 μm^2 was estimated by the conversion from the number of particles per volume. Figure 14 shows the calculated result as a function of oxide radius for various average values of Al decrease in the ADZ. For example, when the average decrease in Al is 0.4 mass pct, several hundreds of oxide particles of diameter 0.2 μm would be precipitated within the ADZ of 1000 μm^2. The calculation results were in reasonable agreement with the experiment results shown in Figure 9. Therefore, it could be considered that the precipitation of Al_2O_3 and $CaO \cdot Al_2O_3$ oxide was positively correlated with the decrease of Al concentration in the alloy near the interface, although this calculation was somewhat approximate.

2. *Dynamic calculation model*
In this study, the method used to produce the diffusion couples was almost the same as that in previous work.[9] The width of the PPZ was determined by the two types of solid-state reaction between Fe-Al-Ca alloy and Al_2O_3-CaO-FeO oxide during heat treatment. Although it might not be completely accurate, the Wagner equation,[18] which was developed to calculate the thickness of the internal oxidation zone in steel, was used to calculate the PPZ width in different diffusion couples in this experiment. The Wagner equation is

$$\xi = \left[\frac{2N_O^{(s)} D_O}{v N_B^{(O)}} t \right]^{1/2}, \quad [14]$$
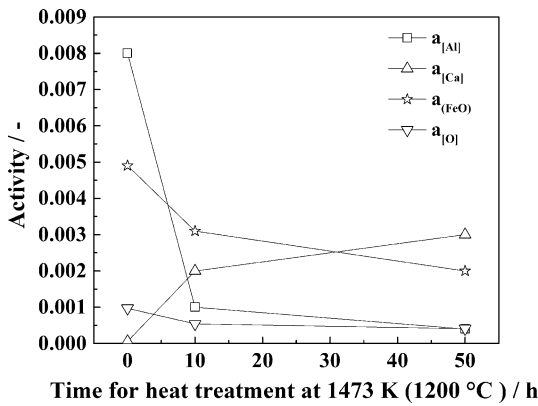
Fig. 13—Activities of Al, Ca, O in the alloy, and FeO in the oxide before and after the heat treatment at 1473 K (1200 °C) for 10 and 50 h.
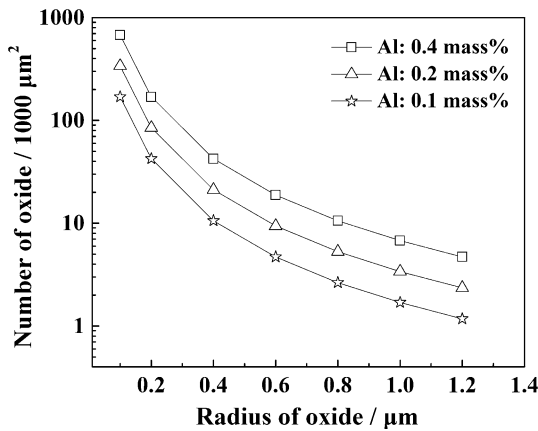

Fig. 14—Density of oxide as a function of oxide radius for various average values of Al decrease in the ADZ by calculation.

where ξ represents the depth of the internal oxidation zone, $N_O^{(s)}$ represents the mole fraction of oxygen in the alloy, D_O indicates the diffusivity of oxygen in the alloy which was calculated by Eq. [15] in γ-iron at each temperature,[19] v is the number of oxygen atoms per A atom in AO_x oxide, $N_B^{(O)}$ is the mole fraction of the solute element in the alloy, and t is reaction time. In this calculation, the method to determine the $N_O^{(s)}$ was similar to that in a previous report.[9] $N_O^{(s)}$ was obtained according to the equilibrium relation between the Fe-Al-Ca alloy and Al_2O_3-CaO-FeO oxide, while v was determined by assuming the formation of pure Al_2O_3 without considering the generation of $CaO \cdot Al_2O_3$ dendritic inclusions. Meanwhile, $N_B^{(O)}$ was calculated according to the composition of Fe-Al-Ca alloy in the diffusion couples.

$$\log D_O = -\frac{8820}{T} + 0.76 \quad [15]$$

Figure 15 shows the change of PPZ with heat treatment time and FeO content before and after heat treatment at 1473 K (1200 °C). In this experiment, prior to heat treatment at 1473 K (1200 °C), the samples were heated
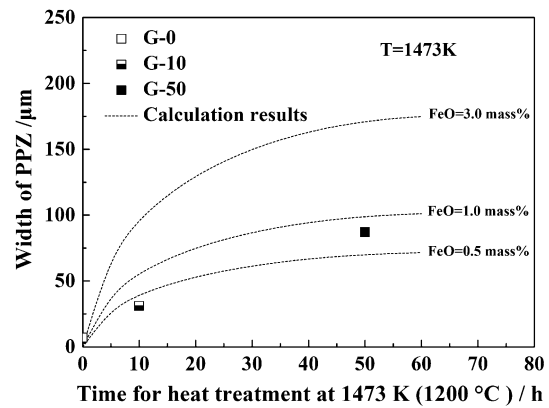

Fig. 15—Change of PPZ width with heat treatment time and FeO content before and after heat treatment at 1473 K (1200 °C).

at 1700 K (1427 °C) to melt the oxide. Therefore, slight reaction between the alloy and oxide occurred, causing the short PPZ width. However, in the calculation, the heating time at 1700 K (1427 °C) was assumed to be 0 seconds, which means the calculated PPZ width was 0 μm in the case of G-0. After heat treatment at 1473 K (1200 °C) for 10 hours, chemical reaction between excess oxygen from the decomposition of FeO in the oxide and Al element in the alloy played a dominant role in determining PPZ width. Experimental results corresponded well with the calculated plot for 0.5 mass pct FeO. However, after heat treatment at 1473 K (1200 °C) for 50 hours, FeO content in the oxide decreased to approximately 0.1 mass pct. The influence of the chemical reaction between FeO and Al on PPZ width was much weakened, while the solid-state reaction between $12CaO \cdot 7Al_2O_3$ in the oxide and Al element in the alloy gradually became the dominant factor determining PPZ width. Figure 15 shows a discrepancy between calculated and experimental values for the diffusion couple G-50. However, the dynamic model used to calculate PPZ width still contributed to understanding the solid-state reactions and element diffusion between Fe-Al-Ca alloy and Al_2O_3-CaO-FeO oxide to some extent.

IV. CONCLUSION

Solid-state reactions between Fe-Al-Ca alloy and Al_2O_3-CaO-FeO oxide during heat treatment at 1473 K (1200 °C) were investigated by a new method using CSLM to produce diffusion couples. The following conclusions can be drawn from the experimental results of this study.

1. The equilibrium oxide with Fe-Al-Ca alloy is not a binary oxide of Al_2O_3-CaO but a ternary oxide containing 0.5 mass pct FeO. As the temperature decreased to 1473 K (1200 °C), the alloy and oxide became non-equilibrated and solid-state reactions occurred between them.
2. After heat treatment at 1473 K (1200 °C), gradual decomposition of FeO in the oxide generated excess oxygen at the interface between the alloy and oxide.

The oxygen diffused into the alloy and reacted with Al, which caused the Al content to decrease and the precipitation of Al_2O_3 particles in the alloy near the alloy–oxide interface.

3. During heat treatment at 1473 K (1200 °C), a solid-state reaction occurred between the $12CaO \cdot 7Al_2O_3$ phase in the oxide and Al element in the alloy, which further promoted the decrease of Al content and increase of Ca content in the alloy. Some $CaO \cdot Al_2O_3$ dendritic inclusions precipitated as reaction products in the alloy near the alloy–oxide interface.

4. PPZ width was determined from the above two types of solid-state reaction between Fe-Al-Ca alloy and Al_2O_3-CaO-FeO oxide. A dynamic model based on the Wagner equation to calculate PPZ width was proposed. This model was helpful to understand the mechanism of solid-state reactions and element diffusion between the alloy and oxide during heat treatment.

REFERENCES

1. Z.H. Wu, W. Zheng, G.Q. Li, H. Matsuura, and F. Tsukihashi: *Metall. Matter. Trans. B*, 2015, vol. 46B, pp. 1226–41.
2. W. Zheng, Z.H. Wu, G.Q. Li, Z. Zhang, and C.Y. Zhu: *ISIJ Int.*, 2014, vol. 54, pp. 1755–64.
3. I. Takahashi, T. Sakae, and T. Yoshida: *Tetsu-to-Hagané*, 1967, vol. 53, pp. 168–70.
4. H. Shibata, T. Tanaka, K. Kimura, and S. Kitamura: *Ironmak. Steelmak.*, 2010, vol. 37, pp. 522–28.
5. H. Shibata, K. Kimura, T. Tanaka, and S. Kitamura: *ISIJ Int.*, 2011, vol. 51, pp. 1944–50.
6. X.J. Shao, X.H. Wang, M. Jiang, W.J. Wang, and F.X. Huang: *ISIJ Int.*, 2011, vol. 51, pp. 1995–2001.
7. W. Choi, H. Matsuura, and F. Tsukihashi: *ISIJ Int.*, 2011, vol. 51, pp. 1951–56.
8. Y. Ohba, Y. Yamashita, K. Ohno, T. Maeda, K. Nishioka, and M. Shimizu: *Tetsu-to-Hagané*, 2009, vol. 95, pp. 531–40.
9. C.S. Liu, K.H. Kim, S.J. Kim, J.S. Li, S. Ueda, X. Gao, H. Shibata, and S. Kitamura: *Metall. Matter. Trans. B*, 2015, vol. 46B, pp. 1875–84.
10. K.H. Kim, S.J. Kim, H. Shibata, and S. Kitamura: *ISIJ Int.*, 2014, vol. 54, pp. 2144–53.
11. J.A. Imlach and F.P. Glasser: *Trans. J. Br. Ceram. Soc.*, 1973, vol. 72, pp. 221–30.
12. V. Espejo and M. Iwase: *Metall. Matter. Trans. B*, 1995, vol. 26B, pp. 257–64.
13. The Japan Institute of Metals: *Physical Chemistry of Metals*, Maruzen Press, Tokyo, 1996, pp. 198–208.
14. E.T. Turkdogan: *Physical Chemistry of High Temperature Technology*, Academic Press, New York, 1980, p. 81.
15. Mitsutaka Hino and Kimihisa Ito: *Thermodynamic Data for Steelmaking*, Tohoku University Press, Sendai, 2010, pp. 5–8.
16. S. Srikanth, V.S. Srinivasan, K.T. Jacob, and M. Allibert: *Rev. Int. Hautes Tempér. Retract.*, 1991, vol. 27, pp. 131–39.
17. S. Ban-ya: *ISIJ Int.*, 1993, vol. 33, pp. 2–11.
18. C. Wagner: *Z. Elektrochem.*, 1959, vol. 63, pp. 772–83.
19. J.H. Swisher and E.T. Turkdogan: *Trans. Met. Soc. AIME*, 1967, vol. 239, pp. 426–31.